Electric Power Systems Research 171 (2019) 54–65

Contents lists available at ScienceDirect

Electric Power Systems Research

journal homepage: www.elsevier.com/locate/epsr

Low-voltage grid behaviour in the presence of concentrated var-sinks and var-compensated customers

Albana Ilo*, Daniel-Leon Schultis

Institute of Energy Systems and Electrical Drives, TU Wien, Vienna, Austria

ARTICLE INFO

Keywords:
Distributed generation
LINK-solution
Low-voltage grid
Operation strategy
Power factor correction
Volt/var control

ABSTRACT

This study investigates the behaviour of low-voltage grids characterised by the maximum presence of prosumers. *LINK*-solution properties are used to select the most suitable voltage control strategy and to simplify the Volt/var management of low voltage grids. DSO-owned concentrated var-sinks, i.e. inductive devices, are set at the end of each feeder whose upper voltage limit is violated. All of the customer-owned PVs inject into the grid by a power factor of unity. Meanwhile, the customer-owned intelligent inverters are used to meet their reactive power requirements at any time. (i.e. they are employed for local power factor correction at the customer sites). Customers act reactive-power-self-sufficient or reactive-power-autarkic. The study is conducted in a theoretical low-voltage grid and four typical real ones: large and small urban, rural, and industrial grids. The results show that the concentrated var-sinks eliminate the violation of upper voltage limit in each case. The reactive-power-autarkic customers release the grid from the reactive power of the load. This means there is no exchange of reactive power between the grid and the customers; the Volt/var management of low-voltage grids can be simplified drastically. Additionally, distribution transformers capacities are released and, for the industrial grid, the capacity release reached 18.61%. Therefore, the existing capacities can be fully utilized and capital expenditures postponed.

1. Introduction

The massive integration of rooftop photovoltaic (PV) facilities challenges the operation of low-voltage grids (LVG), as it causes the violation of upper voltage limit [1]. To eliminate these voltage violations, different measures are proposed like upgrading distribution transformers (DTRs) with on-load tap changers [2], upgrading the customer PV-inverters with different local Volt/var control strategies [3–5], their combination [6] and the combination with active power curtailment [7]. The use of on-load controllable DTRs may control the voltage on the low voltage bus, but cannot guarantee that the voltage will remain within the limits throughout the length of the feeder. Additionally, feeders with low or no PV shares that are supplied by the same DTR may be negatively affected by this action [8]. To avoid these drawbacks, Refs. [6,9,10]. propose to employ a combination of on-load controllable DTRs with a local reactive power, *Q*, control on each existing PV inverter. In this method, distributed data collection and central control are necessary to control the voltage of LVGs with high PV shares. To eliminate the data collection requirement and associated communication issues, it is frequently attempted to solve voltage problems by using different local Volt/var controls [11–20].

Table 1 lists various solutions that have been developed so far to control the reactive power locally. Usually, the active power produced by PVs is variable, as it depends strongly on the weather conditions. Meanwhile, the reactive power contribution of the PV inverters is determined by the distribution grid operator (DSO), with either fixed or variable target values [11]. The latter can be set by remote control, i.e. online pre-setting of target values, or by schedules [12]. The set value may be a constant power factor or reactive power [18,20], constant voltage at a given bus [15], $Q^{inv}(U_{FeederBus})$ characteristic [16,17], or $\cos\varphi^{inv}(P^{inv})$ characteristic [18,19]. These methods are further refined by including more local variables, such as $Q^{inv}(U_{FeederBus}, P^{inv})$ in Ref. [18], $Q^{inv}(P^{inv}, P_{Load}, Q_{Load})$ and $Q^{inv}(P^{inv}, P_{Load}, Q_{Load}$, R/X) in Ref. [13], $\cos\varphi^{inv}(P^{inv}, U_{FeederBus})$ in Refs. [3,15], $\cos\varphi^{inv}(U_{FeederBus})$ [15], and $\cos\varphi^{inv}(P^{inv}$, R/X) in Ref. [16]. Although all of these methods act on local variables, many studies require the use of information and communication technologies (ICT) to coordinate them by sending set points [15,21,22] or certain parameters [14].

LVGs are characterized by the fact that customers' plants are closely to each other, and almost homogeneously connected. In this case, the customers' smart inverters are used to support the grid operation. Fig. 1 presents a schematic of the interaction between the DSO and the

* Corresponding author.
E-mail address: albana.ilo@tuwien.ac.at (A. Ilo).

https://doi.org/10.1016/j.epsr.2019.01.031
Received 18 June 2018; Received in revised form 16 January 2019; Accepted 28 January 2019

Nomenclature

$\cos(\varphi)^{Lo}$	The cos(j) of the load
$\cos(\varphi)^{\mathrm{inv}}$	The cos(j) of the inverter
m	The number of violated buses
n^{dev}	The number of currently supplied devices
n_{Coil}	The number of coils
$n_{Cost..}$	The number of customers
P	The active power
P^{inv}	The active power injected by the inverter
P_{Load}	The active power consumed by the load
$\Delta Q^{DTR+Feeders}$	The reactive power losses in the DTR and feeders
Q	The reactive power
$Q^{dev}(i)$	The reactive power consumed by device i
$Q_{Coil}^{Q-Aut}(j)$	The reactive power consumption of the j coil necessary to keep the voltage under the upper
Q_{CP}^{LV}	The reactive power exchange between the LVG and the customer plant
Q_{ex}^{Q-Aut}	The reactive power flow from the MV_ into the LV_Link-Grid when all of the prosumers are acting Q-Autarkic
Q^{coil}	The reactive power consumption of the coil to mitigate the voltage violation with Q-Autarky
$Q_{Coil}(j)$	The reactive power consumption of coil j, necessary to keep the voltage under the upper limit
Q_{ex}	The reactive power exchange calculated on the primary side of the DTR
Q_{ind}	The reactive power consumption of the coil to mitigate the voltage violation without Q-Autarky
Q^{inv}	The reactive power produced by the inverter
Q_{Load}	The natural reactive power consumption of the load
R/X	The resistance to inductance ratio
*Rel*Cap	The released capacities on distribution transformers
S	The calculated apparent power
S_n	The installed DTR capacity
Δu^{global}	The voltage change caused by the reactive power injection in radial structures
$U_{\mathrm{Coil}}(j)$	The voltage of the bus where is connected the coil j
U^{FdHb}	The voltage of the feeder head bus bar
$U_{FeederBus}$	The voltage of the feeder bus where the inverter is connected
U_{Lo}	The voltage of the load bus
VI	The violation index

customer in the $Q^{inv}(U_{FeederBus})$ operation mode. From Fig. 1 it is clearly to recognize that the LVG operation is intertwined with the operation of each thereto connected inverter, although the latter are the customers' property. The Q provided by the inverters depends on the feeder bus voltage where the house and hence the inverter are connected. Meanwhile, the reactive power consumed by the house electrical devices changes randomly, depending on how many of them are currently in use. Therefore, the total reactive power flow through the intersection point of the customer plant with the LVG is a function of the bus voltage and customer's electrical devices currently in operation.

All of the current solutions intended to prevent upper voltage limit violations cause new technical and social problems. PV inverters in $\cos\varphi^{inv}(P^{inv})$ or $Q^{\mathrm{inv}}(U_{\mathrm{FeederBus}})$ operation mode causes an excessive reactive power flow thus increasing considerably the grid losses and DTRs loading [23] and in many cases active power curtailments are necessary [24] to ensure the quality and reliability of supply. Their coordination provokes major ICT challenges [25], and moreover their resolution is not yet foreseeable. The intertwined operation of inverters, owned by customers, with the LVG causes social problems in the field of discrimination and data privacy.

To overcome the actual social and technical problems, the *LINK*-Paradigm and resulting *LINK*-Solution are used [26]. The *LINK*-Solution stipulates that each grid operator should primarily use its own reactive devices to control the voltage. The use of the concentrated local var-sink (expressed as $L(U)$) control, owned by the DSO, shows clear advantages over the distributed Volt/var local control strategies, realised by customers' inverters [27].

This study investigates the behaviour of low-voltage grids characterised by the maximum presence of prosumers. Firstly, the prerequisites for setting up var-compensated customers are analysed. Secondly, the characteristics of the theoretical and real Link-Grids, and the used methodology are described. In the following, the study results are clearly presented by using graphs and tables. Finally, the possibility to enhance the effectiveness of exploitation of the existing infrastructures is discussed, and the conclusions of this research are given.

Table 1
Smart inverter control modes.

	Operation modes
Current solutions	Variable P, constant power factor
	Variable P, constant reactive power
	Variable P, constant voltage at given bus
	Variable P, variable $\cos\varphi^{\mathrm{inv}}(P^{\mathrm{inv}})$
	Variable P, variable $Q^{\mathrm{inv}}(U_{\mathrm{FeederBus}})$
LINK solution	Variable P, variable $Q^{\mathrm{inv}}(Q_{\mathrm{Load}})$

2. Prerequisites for setting up var-compensated customers

The *LINK*-Solution provides a new approach for the large-scale integration of decentralised generation [28]. For the complete dynamic optimization of power systems, a combination of primary and secondary control is considered. Different Link types, which create the foundation of the unified *LINK*-based architecture of smart power grids, operate as single autonomous systems, while providing the required flexibility by their control schemes. Each of them behaves like a black box and has neither information nor access to the various appliances within the neighbouring links. Therefore, the current smart inverter control solutions presented in Table 1, where the DSO uses the customer-owned appliances to control the voltage in LVGs, are not relevant for the *LINK* solution. For use in this context, we employed the following new control strategy ensemble.

Fig. 2 shows an overview of the low-voltage (LV) and customer plant (CP) Grid-Links (LV_Grid-Link and CP_Grid-Link) in the case of Volt/var control. As per definition, the LV_Grid-Link includes reactive devices such as coils that contribute to the voltage control. The Volt/var secondary control in LV_Grid-Link ($\mathrm{VVSC}^{\mathrm{LV}}$) adapts the primary control settings (e.g. the voltage set point at which to switch on the coil) to the changing operation conditions while respecting the boundary constraints (e.g. the reactive power exchanged with the higher-voltage grid). The concentrated $L(U)$ local control strategy is used to prevent upper voltage limit violation in the LVG [27]. In this case, the DSO uses

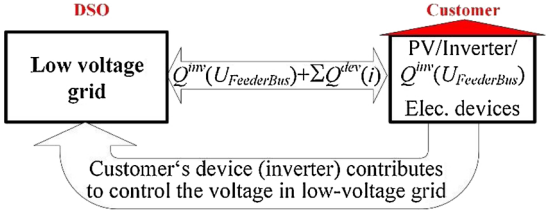

Fig. 1. Schematic of the interaction between the DSO and customer in $Q^{\mathrm{inv}}(U_{\mathrm{FeederBus}})$ operation mode.

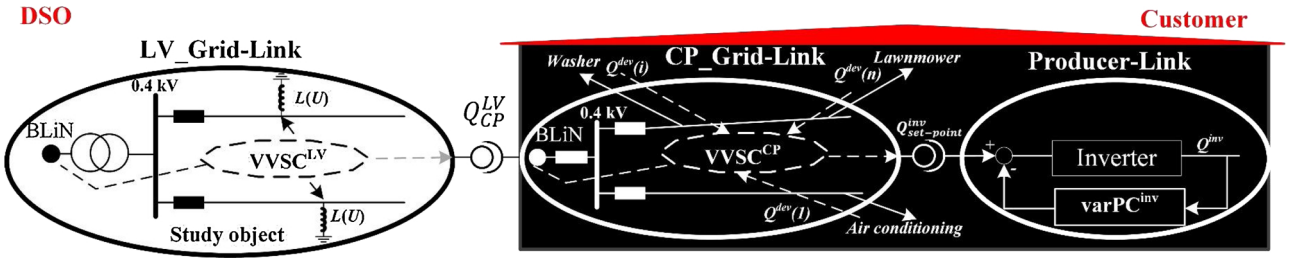

Fig. 2. Overview of the LV_ and CP_Grid-Links in the case of Volt/var control.

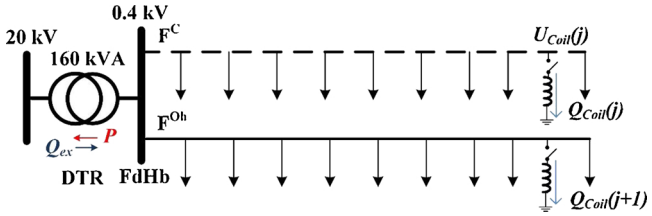

Fig. 3. Schematic of the simplified, theoretical Link-Grid.

its own reactive device, which may be a coil, to control the voltage in its operation area.

The CP_Grid-Link, which represents a prosumer, has a Volt/var secondary control (VVSC^{CP}) over the grid to which the CP devices (including inverter) are connected [26]. The VVSC^{CP} adapts the primary control settings of the inverter var primary control (varPC^{inv}). The reactive power flow between the CP_ and LV-Grid-Link, Q_{CP}^{LV}, can be controlled using the following equation

$$Q_{set-point}^{inv} - \sum_{1}^{n^{dev}} Q^{dev}(i) = Q_{CP}^{LV} \tag{1}$$

where $Q_{set-point}^{inv}$ — reactive power set-point of inverter calculated by VVSC^{CP}; $Q^{dev}(i)$ — reactive power consumed by device i; n^{dev} — number of currently supplied devices; Q_{CP}^{LV} — reactive power exchanged between the LV_ and CP_Grid-Links.

In the special case when

$$Q_{CP}^{LV} = 0 \tag{2}$$

the inverter produces in real time only the reactive power, Q^{inv}, required by the rotating devices, such as washing machines, lawnmowers, air conditioning units, etc. Therefore, the customers are fully compensated and act Q self-sufficient or Q-Autarkic. This means that LVG serves prosumers and consumers by a power factor of unity. In principle, the inverter can exist regardless of the PVs, or, when it is PV-associated, it may be oversized to allow for the necessary reactive power production even at maximal active power injection. However, the description and investigation of VVSC^{CP} and VVSC^{LV} are not the subjects of this paper. Here we focus on the analysis of LVG behaviour when the discussed control strategy ensemble (concentrated local var-sinks and Q-Autarkic customers) is used.

3. Link-Grid characteristics and methodology

The investigations are performed in a theoretical and four real LV_Link-Grids for various control strategies and scenarios. Meanwhile, the results are assessed according to various evaluation entities.

3.1. Investigated LV_Link-Grids

To study the behaviour of LVGs with maximum presence of prosumers, one theoretical and four European real grids are used. The modelling is done based on the assumption of a balanced 3-phase radial configuration. The prosumers in all of the test Link-Grids are characterized by their loads and PV injections. Three different load classes are considered: residential, commercial, and industrial. The loads are modelled based on the active and reactive power consumption. The active power is calculated based on the annual consumption, while the reactive power is derived by using power factors of 0.95, 0.90, and 0.9 for the residential, commercial, and industrial classes, respectively. All of the loads are modelled using an inherent ZIP model [29]. To simulate the largest possible PV penetration, it is supposed that a 5.0 kWp PV facility is installed on every house roof (for more details, see Appendix A). All simulations are performed using NEPLAN.

3.1.1. Theoretical

Fig. 3 presents a schematic of the simplified, theoretical Link-Grid. It consists of two feeders: F^{C} with a cable structure and F^{Oh} with an overhead-line structure connected to the feeder head bus bar (FdHb). They are connected to the MV_Link-Grid through a 20 kV/0.4 kV, 160 kVA DTR. In each feeder, 20 residential customers are connected, Table 2. This Table lists the parameters of the theoretical and real LV_Link-Grids.

3.1.2. Real

To see the effects of the new control strategy on real European LVGs, four different grid types are selected: large and small urban, rural, and industrial. Fig. 4 depicts schematics of the different real LV_Link-Grids. While, their characteristic parameters are summarized in Table 2. Fig. 4(a) and (b) show a simplified one-line diagram of typical large and small urban LV_Link-Grids, with nine and six main feeders, respectively. In the large urban LV_Link-Grid, the longest feeder is 1.27 km long, while in the small urban one, the longest feeder reaches 0.61 km. Both grids have a very high cable share and supply only residential

Table 2
Low-voltage test Link-Grids.

Test grid	DTR		Prosumer number			Feeder length		Feeder number	Cable share [%]
	$\frac{U_1}{U_2}$ [kV/kV]	S_n [kVA]	Res	Com	Ind	Max [km]	Min [km]		
Theoretical	20/0.40	160	40	0	0	1.630	1.630	2	50
Large urban	20/0.40	630	175	0	0	1.270	0.305	9	96
Small urban	21/0.42	400	91	0	0	0.610	0.150	6	81
Rural	20/0.40	160	61	0	0	1.630	0.565	4	59
Industrial	20/0.40	800	7	4	10	0.715	0.025	3	100

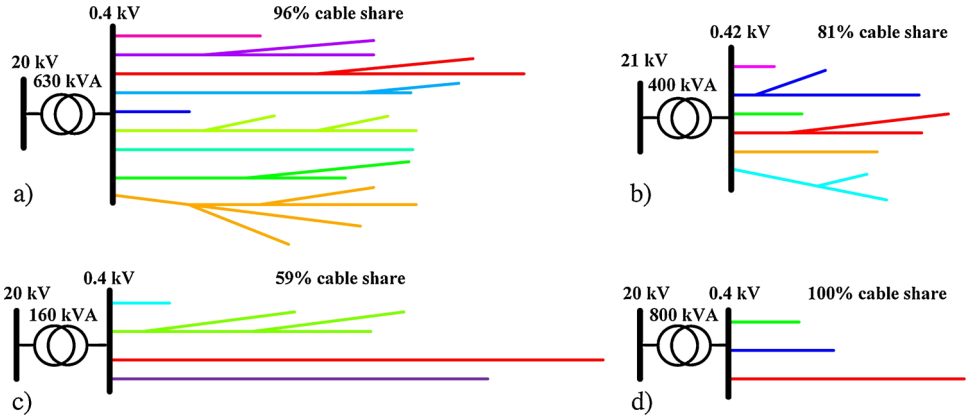

Fig. 4. Schematics of different real LV_Link-Grids: (a) large urban, (b) small urban, (c) rural, and (d) industrial.

customers, 175 and 91 residential customers in large and small urban grids, respectively. Fig. 4(c) shows a simplified one-line diagram of a typical rural LV_Link-Grid with four main feeders. The longest feeder is 1.63 km long. In this grid with a 59% cable share, 61 rural residential customers are connected. Fig. 4(d) depicts a simplified one-line diagram of a typical industrial LV_Link-Grid with three main feeders. The longest feeder is 0.715 km long. In this grid with a 100% cable structure, seven residential, four commercial, and ten industrial customers are connected.

3.2. Methodology

3.2.1. Control strategies

Three different cases are considered:

- No control applied (the upper voltage limit is violated);
- $L(U)$ voltage control applied at the end of each violated feeder. The var-sinks are modelled as shunt coils switched on for $U_{\mathrm{Coil}}(j) > 1.09$ p.u. Where $U_{\mathrm{Coil}}(j)$ is the bus voltage where the coil j is connected. In this case this bus behaves as a PV node;
- $L(U)$ control and prosumers operating Q-Autarkic.

3.2.2. Simulation scenarios

The voltage behaviour of the different LV_Link-Grids is investigated for the worst case with respect to voltage violations: minimal load and maximum PV production, $L^{\min}$–$P^{\max}$.

To investigate losses, DTR loading and released capacities, additional Load/Production scenarios are considered such as: minimal load and minimal PV production, $L^{\min}$–$P^{\min}$; maximum load and minimal PV production, $L^{\max}$–$P^{\min}$; minimal load and middle PV production, $L^{\min}$–P^{mid}; maximum load and middle PV production, $L^{\max}$–P^{mid}; maximal load and maximal PV production, $L^{\max}$–$P^{\max}$.

In all cases, the upper voltage limit is set to 1.1 p.u.

3.2.3. Evaluation entities

The following entities are used to evaluate the behaviour of the LV_Link-Grids:

- Number of violated feeders and buses;
- Violation index VI, which is calculated using

$$VI = \frac{\sum_{i=1}^{m} (U^{viol}(i) - U_{lim}^{upper}}{m \cdot U_{lim}^{upper}}, \tag{3}$$

where m — number of violated buses, U^{viol}— voltage of the violated bus, U_{lim}^{upper}— upper voltage limit;

- Losses — grid and DTR losses;
- Reactive power exchange, Q_{ex}, calculated on the primary side of the DTR;
- DTR loading;
- Global voltage change as result of the reactive power injection on the radial structures [30] as in

$$\Delta u^{global}(GridType) = U_{NoCtrl}^{FdHb}(GridType) - U_{Ctrl(j)}^{FdHb}(GridType), \tag{4}$$

where the Grid Type may be large or small urban, rural or industrial, U_{NoCtrl}^{FdHb} — voltage on the FdHb when no control is applied, $U_{Ctrl(j)}^{FdHb}$ — voltage on the FdHb when one of the control strategies $L(U)$ or $L(U)$ combined with Q-Autarky is applied.

4. Steady-state behaviour of LV_Link-Grids

4.1. Two-bus system

The effect of Q-Autarky is firstly discussed in a simple two-bus system with the $L(U)$ control strategy applied. Fig. 5(a) provides a schematic of the two-bus system with an impedance connected in between the feeder head bus, F, and the load bus, Lo. To the latter, a load, a PV facility and a coil are connected. The PV injects into the grid with

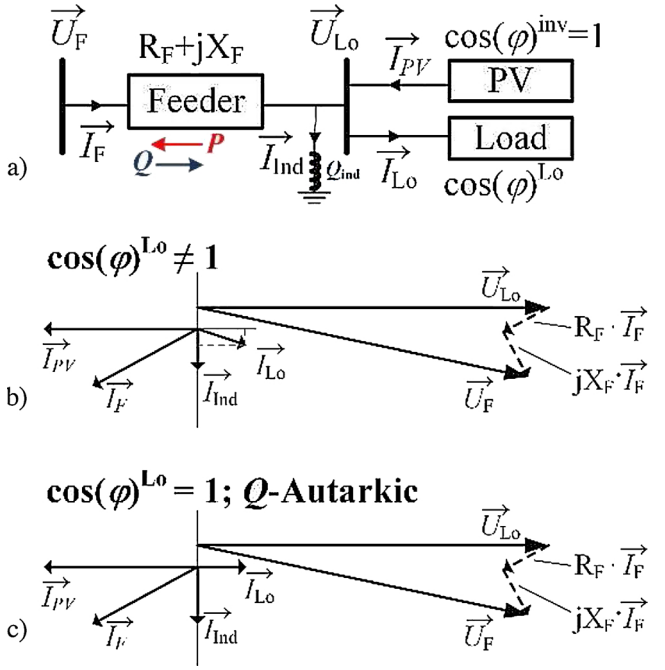

Fig. 5. Two-bus system with feeder impedance, coil control, and PV injection by $\cos(\phi)^{PV} = 1$: (a) schematic, (b) vector diagram for $\cos(\phi)^{Lo} \neq 1$, and (c) vector diagram for $\cos(\phi)^{Lo} = 1$.

$\cos(\phi)^{inv} = 1$, while the load is inductive and consumes power with $\cos(\phi)^{Lo} \neq 1$. The corresponding vector diagram is shown in Fig. 5(b). The active power, P, flows back through the feeder impedance into the feeder head bus bar. While, the reactive power Q flows through the feeder to the load. Normally, the voltage, U_{Lo}, of the bus connecting the PV increases and can exceed the upper voltage limit. To mitigate this voltage violation the coil consumes the reactive power, Q_{ind} as follows:

$$Q^{coil} = Q_{ind}. \tag{5}$$

Fig. 5(c) show the vector diagram when Q-Autarky is applied, $\cos(\phi)^{Lo} = 1$. That means, the customer does not draw reactive power from the feeder. To keep the same U_{Lo} as before, the coil consumption increases by Q_{Load}:

$$Q^{coil} = Q_{ind} + Q_{Load}. \tag{6}$$

The reactive power consumption of the coil increases while the Q-flow through the feeder remains unchanged.

4.2. Theoretical LV_Link-Grid

Fig. 6 shows the voltage profiles of the theoretical Link-Grid with the total minimal load of 27.36 kW and maximal PV injection of 200 kW for different control strategies. The L^{min}–P^{max} scenario is simulated, with each individual load consumption set to 0.684 kW with $\cos(\phi) = 0.95$. Fig. 6(a) shows the voltage profiles of both feeders, F^{C} and F^{Oh}, that are acquired without applying any control. An active power of 153.46 kW flowed from the LV_Link-Grid into the MV_Link-Grid, while a reactive power of 30.07 kvar flowed from the MV_Link-Grid into the LV_Link-Grid (Table 3). The total losses are 15.55 kW, while the DTR exhibits 92.2% loading. The natural reactive power consumption of the consumers is not sufficient to mitigate the voltage violation resulting from the reverse active power flow. Thus, 24 F^{Oh} buses violated the upper voltage limit, with $VI = 0.0595$, while only 23 F^{C} buses violated it, with $VI = 0.0365$. The higher VI of F^{Oh} is related to the impedances of the feeder with the overhead-line structure being higher than those of the feeder with the cable structure. To eliminate the voltage violations, $L(U)$ control is applied. Fig. 6(b) shows the voltage profiles obtained for both F^{C} and F^{Oh} when a $L(U)$ control is set at the end of each violated feeder. The black and grey curves correspond to the cases without and with Q-Autarkic prosumers, respectively. The voltage violations are eliminated in both cases, yielding $VI = 0$. The results demonstrate that the total load compensation does not significantly impact the resulting voltage profile. Fig. 6(c) shows the details of the voltage profiles in the area with the largest voltage difference. This voltage difference reaches a maximum of 0.003 p.u.

Without Q-Autarkic prosumers, the coils connected to F^{C} and F^{Oh} absorbed 57.65 kvar and 24.26 kvar, respectively. An active power of 144.84 kW flowed from the LV_Link-Grid into the MV_Link-Grid, while a reactive power of 118.09 kvar flowed from the MV_Link-Grid into the LV_Link-Grid. Fig. 7(a) presents schematically the active and reactive power flow in the low voltage feeder with the highest PV penetration injecting with $\cos(\phi) = 1$, where the $L(U)$ control strategy is used. The total losses are 25.79 kW, while the DTR shows 110.19% loading. In this case, the reactive power exchange has three components, as in:

Table 3
P, Q, and losses for different control strategies.

	P [kW]	Q [kvar]	Losses [kW]	$DTR^{Loading}$ [%]
No control	153.46	−30.07	15.55	92.2
$L(U)$	144.84	−118.09	25.79	110.19
$L(U)$ + Q-autarky	144.85	−114.67	25.74	108.95

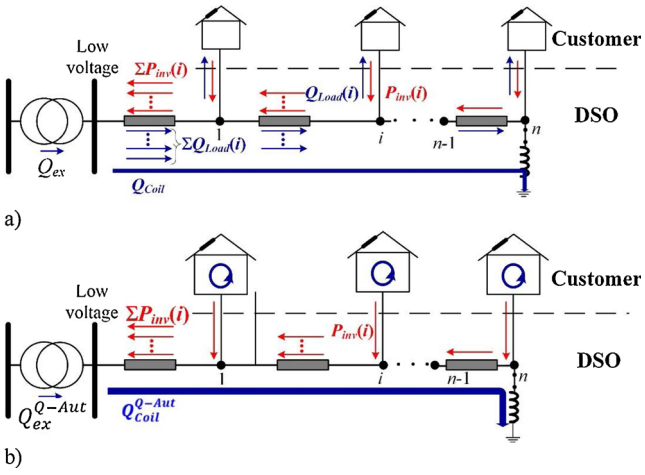

Fig. 7. Active and reactive power flow in a low-voltage feeder with the highest PV penetration that injects with $\cos(\phi) = 1$ and the $L(U)$ control strategy is employed when (a) the reactive power required by the load is supplied by the grid and (b) Q-autarky is applied.

$$Q_{ex} = \sum_{i=1}^{n_{Cust.}} Q_{Load}(i) + \sum_{j=1}^{n_{Coil}} Q_{Coil}(j) + \Delta Q^{DTR+Feeders} \tag{7}$$

where $Q_{Load}(i)$ — natural reactive power consumption of load i; $n_{Cust.}$ — number of customers; $Q_{Coil}(j)$ — reactive power consumption of coil j, necessary to keep the voltage under the upper limit; n_{Coil} — number of coils; $\Delta Q^{DTR+Feeders}$ — reactive power losses in the DTR and feeders.

With Q-Autarkic prosumers, the coils connected at F^{C} and F^{Oh} absorbed 61.95 kvar and 28.10 kvar, respectively. An active power of 144.85 kW flowed from the LV_Link-Grid into the MV_Link-Grid, while a reactive power of 114.67 kvar flowed from the MV_Link-Grid into the LV_Link-Grid, Table 3. In this case, the reactive power exchange had only two components, as shown in Fig. 7(b) and expressed in:

$$Q_{ex}^{Q-Aut} = \sum_{j=1}^{n_{Coil}} Q_{Coil}^{Q-Aut}(j) + \Delta Q^{DTR+Feeders} \tag{8}$$

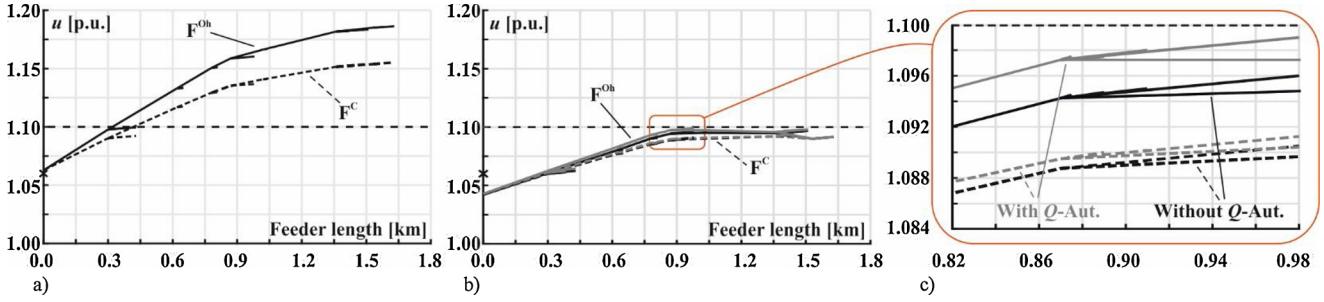

Fig. 6. Voltage profiles of the theoretical Link-Grid for a minimal load of 54.72 kW and maximal PV injection of 200 kW for different control strategies: (a) no control, (b) $L(U)$ control with and without Q-Autarkic prosumer, and (c) detailed view.

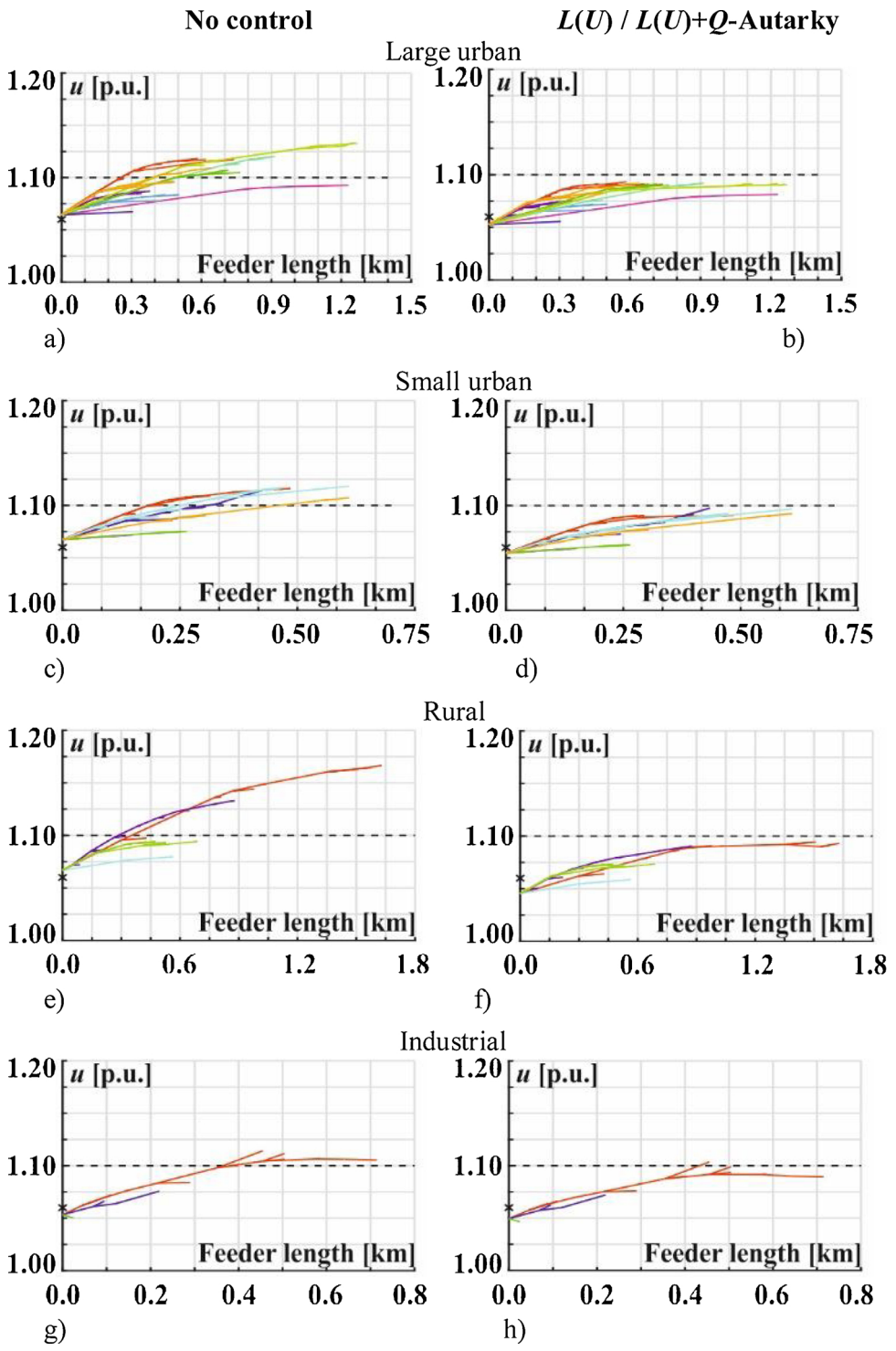

Fig. 8. Overview of the voltage profiles of four typical real Link-Grids for the minimal load and maximal PV injection with no, $L(U)$, or $L(U)+Q$-Autarky control.

Table 4
Large urban Link-Grid results for minimal load (171 kW) and maximal PV-injection (875 kW).

Control strategy	Number of violated		*VI*	Losses [kW]	Q_{ex} [kvar]	$DTR^{Loading}$ [%]	Δu^{global} [p.u.]
	Feeders	Buses					
None	5	112	0.0122	29.38	106.19	100.04	–
$L(U)$	0	0	0.0000	41.13	309.2	107.88	0.0118
$L(U)$ and Q_{Aut}	0	0	0.0000	41.91	288.61	106.47	0.0106

Table 5
Small urban Link-Grid results for minimal load (119 kW) and maximal PV-injection (728 kW).

Control strategy	Number of violated		*VI*	Losses [kW]	Q_{ex} [kvar]	$DTR^{Loading}$ [%]	Δu^{global} [p.u.]
	Feeders	Buses					
none	4	58	0.0085	24.70	87.23	137.63	–
$L(U)$	0	0	0.0000	31.09	240.62	146.54	0.0128
$L(U)$ and Q_{Aut}	0	0	0.0000	31.60	232.05	145.64	0.0121

Table 6
Rural Link-Grid results for minimal load (42 kW) and maximal PV-injection (305 kW).

Control strategy	Number of violated		*VI*	Losses [kW]	Q_{ex} [kvar]	$DTR^{Loading}$ [%]	Δu^{global} [p.u.]
	Feeders	Buses					
None	2	42	0.0347	15.35	39.82	146.22	–
L(U)	0	0	0.0000	25.96	131.32	159.2	0.0214
$L(U)$ and Q_{Aut}	0	0	0.0000	26.15	124.40	157.11	0.0199

Table 7
Industrial Link-Grid Results for minimal load (391 kW) and maximal PV-injection (720 kW).

Control strategy	Number of violated		*VI*	Losses [kW]	Q_{ex} [kvar]	$DTR^{Loading}$ [%]	Δu^{global} [p.u.]
	Feeders	Buses					
None	1	9	0.0063	18.63	222.81	42.99	–
$L(U)$	1	1	0.0032	24.01	306.46	49.37	0.0038
$L(U)$ and Q_{Aut}	1	1	0.0036	25.52	170.97	38.75	0.0023

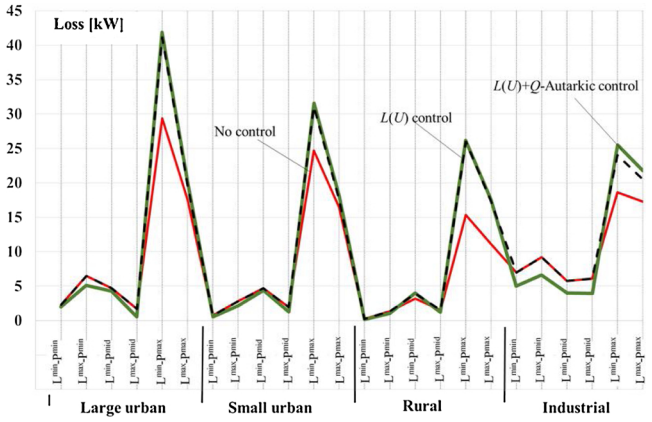

Fig. 9. Losses in different types of real LV_Link-Grids and different scenarios and with different control strategies.

where Q_{ex}^{Q-Aut} — reactive power flow from the MV_Link-Grid into the LV_Link-Grid when all of the prosumers are acting *Q*-Autarkic; $Q_{Coil}^{Q-Aut}(j)$ — reactive power consumption of the coil necessary to keep the voltage under the upper limit when all of the prosumers are acting *Q*-Autarkic.

The total losses are 25.74 kW, while the DTR shows 108.93% loading.

Consequently, applying the $L(U)$ control strategy at the end of each feeder exhibiting an upper voltage limit violation eliminates all of the voltage violations. The DTR loading is 17.98% greater than that in the case with no control. The combination of the $L(U)$ control strategy with *Q*-Autarkic consumers decreases the reactive power flow as follows:

$$Q_{ex} = 118.09\text{kvar} > Q_{ex}^{Q-Aut} = 114.67\text{kvar}. \quad (9)$$

Here, it is very interesting to note that distributed natural reactive power consumption of the loads yields a voltage reduction effect lower than that of concentrated reactive power consumption at the end of the feeder. The DTR capacity is released by 1.24% when the consumers act *Q*-Autarkic.

In principle, in the case of a voltage rise along the feeder, having an inductive load especially close to the end of it helps to mitigate the voltage increase. However, since the load profile does not always coincide with the PV production profile, the reactive power consumption of the loads cannot be considered for the voltage control. Therefore, the customers' *Q*-Autarky shows advantages also in this case.

In this control strategy ensemble, the reactive power devices (e.g. coils), which are under the utility administration, enable unrestricted operation, which does not require any data exchange between the DSO and prosumers. Additionally, enabling the prosumers to act *Q*-Autarkic releases capacity and simplifies the LVG state estimation and Volt/var management. To highlight the effectiveness of the $L(U)$ control strategy and its combination with *Q*-Autarkic prosumers, simulations are also conducted for four typical real LV_Link-Grids.

4.3. European real LV_Link-Grids

The behaviour of the real LV_Link-Grids is also analysed considering the $L^{\min}$-$P^{\max}$ scenario, as most upper voltage limit violations occur in this situation. The slack is always set on the bus of the primary side of the DTR at 1.06 p.u. (shown with "x" on the ordinate axis in each diagram). This voltage value characterises DTRs being connected at the end of the medium voltage feeder.

Fig. 8 shows the voltage profiles of four typical real Link-Grids with minimal loads and maximal PV injections when no, $L(U)$, or $L(U)+Q$-Autarkic control is applied. Different colours are used to draw the voltage profile of various feeders. Different feeders The L(U) control is set at the end of the main branch of each violated feeder. Just as in the case of the theoretical LV_Link-Grid discussed in Section 4.1, the Q-Autarky of the prosumers had no significant impact on the voltage

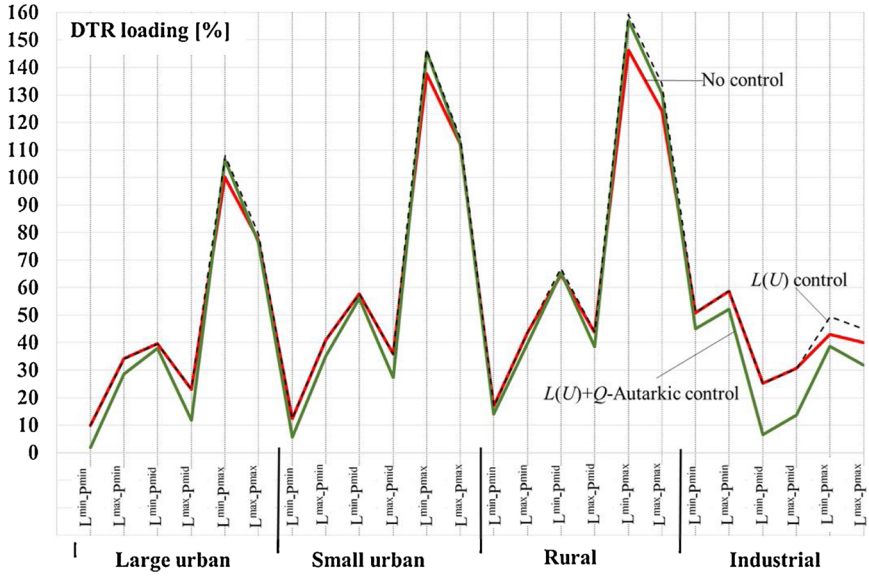

Fig. 10. DTR loading in different types of real LV_Link-Grids and different scenarios and with different control strategies.

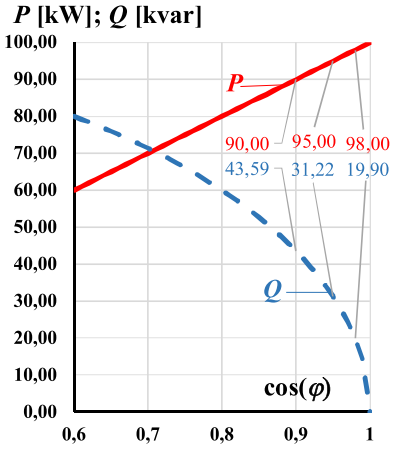

Fig. 11. Effect of the power factor on the reactive power requirements of a 100 kVA load.

profiles of the real LV_Link-Grids. Therefore, the voltage profiles corresponding to the $L(U)$ and $L(U)+Q$-Autarky control cases are not shown separately. However, the other parameters such as number of violated feeders and buses, *VI*, losses, Q_{ex}, $DTR^{Loading}$, and Δu^{global} are influenced by the *Q*-Autarkic operation mode of the prosumers. The voltage of the secondary bus of the DTR shifts in all of the control cases. The simulation results of all of the real LV_Link-Grids are shown in the Tables 4–7.

Fig. 8(a) and (b) show the voltage profiles of all feeders of the large urban LV_Link-Grid with the minimal load, 171.15 kW, and maximal PV injection, 875.0 kW, with no, $L(U)$ and $L(U)+Q$-Autarky control applied. While, Table 4 summarises the simulation results described above. Fig. 8(a) corresponds to the no control case. The number of limit violations is considerable: five feeders, 112 buses are violated with VI = 0.012. The losses reach 29.38 kW. Fig. 8(b) shows the voltage profiles obtained with $L(U)$ or $L(U)+Q$-Autarky control applied. The voltage violations are eliminated in both cases; hence, VI = 0. In both cases, all four parameters (i.e. losses, Q_{ex}, $DTR^{Loading}$, and Δu^{global}) increase with respect to the case with no control. However, with $L(U)+Q$-Autarky, these parameters increase less than in the case of the $L(U)$ control strategy.

Fig. 8(c) and (d) present the voltage profiles of all of the feeders in the small urban LV_Link-Grid with the minimal load, 119 kW, and maximal PV injection, 728.0 kW with no, and $L(U)$ and $L(U)+Q$-Autarky control applied. While, Table 5 summarises the relevant simulation results mentioned above. Fig. 8(c) corresponds to the no control case. The upper voltage limit is violated by four feeders, by 58 buses with VI = 0.0085. The losses reach 24.70 kW. Fig. 8(d) shows the voltage profiles obtained with $L(U)$ or $L(U)+Q$-Autarky control applied. Similar to the large urban Link-Grid, the voltage violations are eliminated in both cases; hence, VI = 0. As with the large urban grid, the same tendency is observed with respect to the four parameters (losses, Q_{ex}, $DTR^{Loading}$, and Δu^{global}).

The same trend is observed for the rural and industrial Link-Grid case as well, as it can be seen in Fig. 8(e)–(h), and in the corresponding Tables 6 and 7 respectively.

In order to check this trend for other operating conditions as well, various Load/Production scenarios are analysed as follows.

4.4. Released capacities

Fig. 9 depicts the losses obtained with the different real LV_Link-Grid types in various Load/Production scenarios and with no, $L(U)$, or $L(U)+Q$-Autarky control applied. The losses for the large urban and industrial Link-Grids and the L^{min}–P^{min}, L^{max}–P^{min}, L^{min}–P^{mid}, and L^{max}–P^{mid} Load/Production scenarios are smaller with the $L(U)+Q$-Autarky control strategy than with no or $L(U)$ control. In these cases, the reactive power required by the loads is higher than the reactive power needed to keep the voltages within the limits. With the increasing PV-injection in the L^{min}–P^{max} and L^{max}–P^{max} cases, the amount of reactive power needed to eliminate voltage violations increases and thus losses do as well. The $L(U)+Q$-Autarky control strategy decreases the losses by 22.4% for the rural Link-Grid but increases it by 5.9% for the industrial Link-Grid. For the large and small urban Link-Grids, the losses remain almost the same.

Fig. 10 shows the DTR loading in the different real LV_Link-Grid types for different Load/Production scenarios and with no, $L(U)$, or $L(U)+Q$-autarky control. Compared to the $L(U)$ control case, the use of $L(U)+Q$-Autarky control decreases the DTR loading for all of the Load/Production scenarios and for all of the real Link-Grid types. The degree to which the loading decreases depends on the load nature. In the

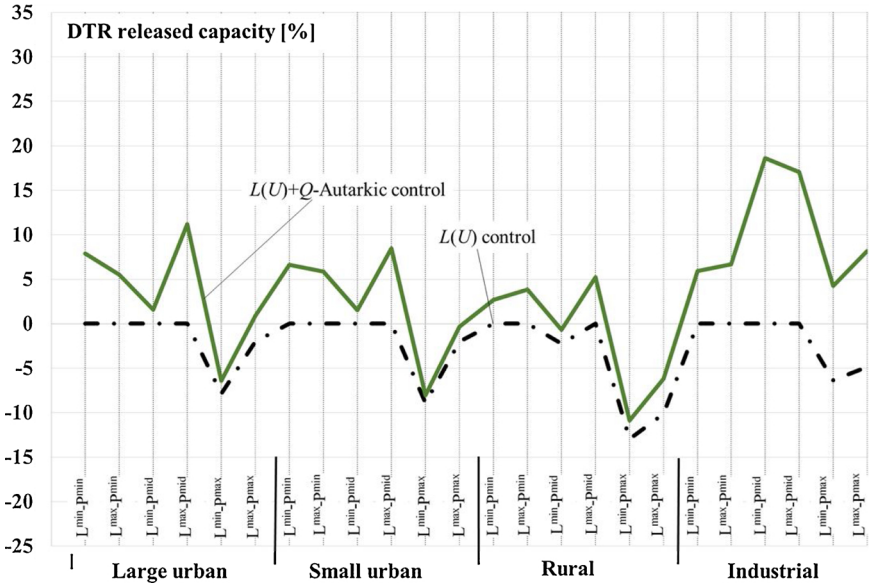

Fig. 12. Released capacity of DTR in different types of real LV_Link-Grids and different scenarios and with different control strategies.

industrial Link-Grid case, the industrial and commercial customers are modelled with cos(ϕ) = 0.9 and therefore it requires a large share of the reactive power, specifically, 43.59% of the total consumed power. Fig. 11 shows the effect of the power factor on the reactive power requirement of a 100 kVA load as an example. The *Q*-curve shows that small cos(ϕ) variations cause very high reactive power changes when the power factor is high. Thus, very different reactive power flows are required by the same load with power factors of 0.98, 0.95, and 0.90, which are respectively 19.90 kvar, 31.22 kvar, and 43.59 kvar or 19.9%, 31.22%, and 43.59%, respectively, of the total load.

Fig. 12 shows the released capacities (RelCap) of the DTR for the different real LV_Link-Grid types, Load/Production scenarios, and control strategies. RelCap is calculated in the $L(U)$ and $L(U)+Q$-Autarkic control cases as follows:

$$RelCap^{Ctrl(j)}(k,\ l) = \left(\frac{S^{NoCtrl}(k,\ l)}{S_n(k)} - \frac{S^{Ctrl(j)}(k,\ l)}{S_n(k)}\right)\bullet 100 \quad (10)$$

where k — one of the real LV_Link-Grids, i.e. large urban, small urban, rural, or industrial; l — one of the Load/Production scenarios; S_n — installed capacity of the DTR; S^{NoCtrl} — calculated apparent power of the DTR when no control is applied; S^{Ctrl}(j) — calculated apparent power of the DTR when one of the control strategies $L(U)$ or $L(U)$ combined with *Q*-Autarky is applied.

The results shows that for L^{min}–P^{min}, L^{max}–P^{min}, L^{min}–P^{mid}, and L^{max}–P^{mid} operation in all of the real LV_Link-Grids, the use of $L(U)$ control does not release the capacities of the DTRs. During high production periods, in the L^{min}-P^{max} and L^{max}-P^{max} scenarios, even more capacity (up to −12.98% for the rural LV_Link-Grid) is needed, but all the upper voltage limit violations are eliminated.

The $L(U)+Q$-Autarky control strategy provides significant advantages in all of the scenarios for all of the studied real LV_Link-Grids. During low production periods, specifically, in the L^{min}–P^{min}, L^{max}–P^{min}, L^{min}–P^{mid}, and L^{max}–P^{mid} scenarios, less DTR capacity (up to 18.61% for the industrial Link-Grid) is required. During high production periods, specifically, in the L^{min}–P^{max} and L^{max}–P^{max} scenarios, more DTR capacity (up to −10.89% for the rural Link-Grid) is required within the large urban, small urban, and rural link grids, while less DTR capacity (up to 4.24%) is required within the industrial link grid.

The results show that the $L(U)+Q$-Autarky control strategy enables more effective use of the existing capacity than the $L(U)$ control strategy. Previous comparative studies of different existing control strategies in LVGs have underlined the benefits of the proposed control strategy [23].

5. Conclusion

The $L(U)$ control strategy eliminates the upper voltage limit violations caused by reverse active power flow. The control strategy ensemble, $L(U)+Q$-Autarky, provides substantial benefits. Specifically, this strategy unloads the grid from the reactive power flow of the load, enabling full utilization of the existing infrastructures and postponement of capital expenditures. Furthermore, the exchange of information between DSOs and prosumers is reduced because DSOs use their own inductive devices for the voltage control in LVGs. This greatly simplifies their Volt/var management tasks.

The basic principle of the proposed method is to replace the local distributed $Q(U)$ control strategy with the $L(U)+Q$-Autarky control ensemble. The special feature of the latter is that the prosumers operate self-sufficient concerning the reactive power. They constantly meet their own reactive power needs, regardless of the voltage behaviour at the connection point.

A practical implementation of the $L(U)$-control strategy (via coils or inverters) will be needed to underline the effectiveness of this method. Similarly to $Q(U)$ control, *Q*-Autarky control is a type of behind-the-meter reactive power control. Therefore, the prosumer's incentives to apply this method in practice should be carefully analysed.

Acknowledgments

This work was supported by TU Wien. We thank our colleague Christian Schirmer for providing the real networks, insights and expertise that greatly assisted the research.

Appendix A

See Fig. 13, Table 8, Table 9.

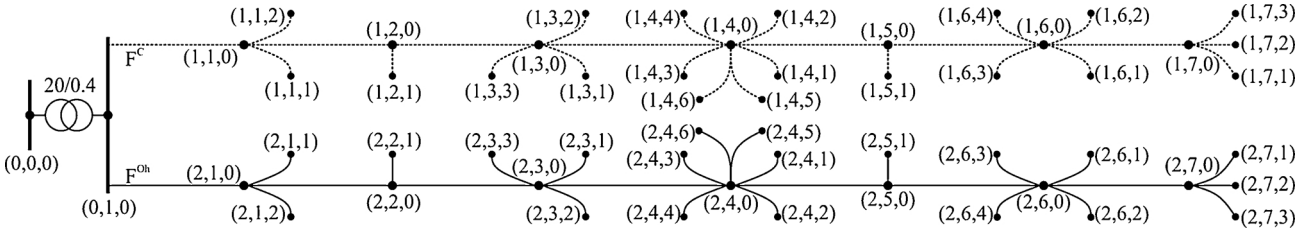

Fig. 13. Details of the theoretical grid.

Table 8
Theoretical grid branch data.

		Input data			Results	
Branch	Branch type	R [mΩ]	X [mΩ]	B [μS]	P [kW]	Q [kvar]
(0,0,0)–(0,1,0)	Trafo	10.000	39.100	0.00	−153.461	30.069
(0,1,0)–(1,1,0)	Cable	61.800	24.000	15.60	−78.995	8.537
(1,1,0)–(1,1,1)	Cable	48.075	6.375	2.70	−4.259	0.283
(1,1,0)–(1,1,2)	Cable	83.330	11.050	4.68	−4.255	0.282
(1,1,0)–(1,2,0)	Cable	65.920	25.600	16.64	−72.640	7.151
(1,2,0)–(1,2,1)	Cable	19.230	2.550	1.08	−4.245	0.306
(1,2,0)–(1,3,0)	Cable	32.960	12.800	8.32	−70.241	6.148
(1,3,0)–(1,3,1)	Cable	6.410	0.850	0.36	−4.238	0.318
(1,3,0)–(1,3,2)	Cable	19.230	2.550	1.08	−4.237	0.318
(1,3,0)–(1,3,3)	Cable	9.615	1.275	0.54	−4.238	0.318
(1,3,0)–(1,4,0)	Cable	18.540	7.200	4.68	−58.350	4.886
(1,4,0)–(1,4,1)	Cable	3.205	0.425	0.18	−4.234	0.323
(1,4,0)–(1,4,2)	Cable	3.205	0.425	0.18	−4.234	0.323
(1,4,0)–(1,4,3)	Cable	70.510	9.350	3.96	−4.227	0.321
(1,4,0)–(1,4,4)	Cable	12.820	1.700	0.72	−4.232	0.323
(1,4,0)–(1,4,5)	Cable	25.640	3.400	1.44	−4.233	0.323
(1,4,0)–(1,4,6)	Cable	3.205	0.425	0.18	−4.234	0.323
(1,4,0)–(1,5,0)	Cable	30.900	12.000	7.80	−33.265	2.834
(1,5,0)–(1,5,1)	Cable	12.820	1.700	0.72	−4.230	0.328
(1,5,0)–(1,6,0)	Cable	70.040	27.200	17.68	−29.203	2.451
(1,6,0)–(1,6,1)	Cable	64.100	8.500	3.60	−4.217	0.336
(1,6,0)–(1,6,2)	Cable	96.150	12.750	5.40	−4.214	0.335
(1,6,0)–(1,6,3)	Cable	38.460	5.100	2.16	−4.219	0.337
(1,6,0)–(1,6,4)	Cable	83.330	11.050	4.68	−4.215	0.336
(1,6,0)–(1,7,0)	Cable	35.020	13.600	8.84	−12.627	1.018
(1,7,0)–(1,7,1)	Cable	64.100	8.500	3.60	−4.215	0.339
(1,7,0)–(1,7,2)	Cable	12.820	1.700	0.72	−4.220	0.341
(1,7,0)–(1,7,3)	Cable	32.050	4.250	1.80	−4.218	0.340
(0,1,0)–(2,1,0)	Line	97.920	106.710	0.00	−75.826	16.208
(2,1,0)–(2,1,1)	Line	46.140	28.230	0.00	−4.255	0.295
(2,1,0)–(2,1,2)	Line	79.976	48.932	0.00	−4.251	0.297
(2,1,0)–(2,2,0)	Line	104.448	113.824	0.00	−70.578	12.067
(2,2,0)–(2,2,1)	Line	18.456	11.292	0.00	−4.234	0.323
(2,2,0)–(2,3,0)	Line	52.224	56.912	0.00	−69.121	8.717
(2,3,0)–(2,3,1)	Line	6.152	3.764	0.00	−4.223	0.339
(2,3,0)–(2,3,2)	Line	18.456	11.292	0.00	−4.222	0.339
(2,3,0)–(2,3,3)	Line	9.228	5.646	0.00	−4.223	0.339
(2,3,0)–(2,4,0)	Line	29.376	32.013	0.00	−57.687	6.356
(2,4,0)–(2,4,1)	Line	3.076	1.882	0.00	−4.218	0.346
(2,4,0)–(2,4,2)	Line	3.076	1.882	0.00	−4.218	0.346
(2,4,0)–(2,4,3)	Line	67.672	41.404	0.00	−4.211	0.351
(2,4,0)–(2,4,4)	Line	12.304	7.528	0.00	−4.217	0.347
(2,4,0)–(2,4,5)	Line	24.608	15.056	0.00	−4.216	0.348
(2,4,0)–(2,4,6)	Line	3.076	1.882	0.00	−4.218	0.346
(2,4,0)–(2,5,0)	Line	48.960	53.355	0.00	−32.857	3.762
(2,5,0)–(2,5,1)	Line	12.304	7.528	0.00	−4.211	0.355
(2,5,0)–(2,6,0)	Line	110.976	120.938	0.00	−28.895	3.136
(2,6,0)–(2,6,1)	Line	61.520	37.640	0.00	−4.195	0.374
(2,6,0)–(2,6,2)	Line	92.280	56.460	0.00	−4.192	0.376
(2,6,0) – (2,6,3)	Line	36.912	22.584	0.00	−4.198	0.372
(2,6,0) – (2,6,4)	Line	79.976	48.932	0.00	−4.194	0.375
(2,6,0) – (2,7,0)	Line	55.488	60.469	0.00	−12.547	1.169
(2,7,0) – (2,7,1)	Line	61.520	37.640	0.00	−4.193	0.377
(2,7,0) – (2,7,2)	Line	12.304	7.528	0.00	−4.197	0.374
(2,7,0) – (2,7,3)	Line	30.760	18.820	0.00	−4.196	0.375

Table 9
Theoretical grid node data.

	Input data	Results	
Node	Load/prod. [kW; kvar]	Load/prod. [kW; kvar]	Volt [kV]
(0,0,0)	–	–	21.2000
(0,1,0)	0.0000; 0.0000	0.000; 0.000	0.4251
(1,1,0)	0.0000; 0.0000	0.000; 0.000	0.4361
(1,1,1)	−4.3160; 0.2248	−4.264; 0.286	0.4366
(1,1,2)	−4.3160; 0.2248	−4.263; 0.286	0.4369
(1,2,0)	0.0000; 0.0000	0.000; 0.000	0.4467
(1,2,1)	−4.3160; 0.2248	−4.247; 0.308	0.4469
(1,3,0)	0.0000; 0.0000	0.000; 0.000	0.4517
(1,3,1)	−4.3160; 0.2248	−4.239; 0.318	0.4518
(1,3,2)	−4.3160; 0.2248	−4.238; 0.319	0.4519
(1,3,3)	−4.3160; 0.2248	−4.238; 0.319	0.4518
(1,4,0)	0.0000; 0.0000	0.000; 0.000	0.4541
(1,4,1)	−4.3160; 0.2248	−4.235; 0.324	0.4541
(1,4,2)	−4.3160; 0.2248	−4.235; 0.324	0.4541
(1,4,3)	−4.3160; 0.2248	−4.234; 0.325	0.4547
(1,4,4)	−4.3160; 0.2248	−4.234; 0.324	0.4542
(1,4,5)	−4.3160; 0.2248	−4.234; 0.324	0.4543
(1,4,6)	−4.3160; 0.2248	−4.235; 0.324	0.4541
(1,5,0)	0.0000; 0.0000	0.000; 0.000	0.4563
(1,5,1)	−4.3160; 0.2248	−4.231; 0.329	0.4564
(1,6,0)	0.0000; 0.0000	0.000; 0.000	0.4606
(1,6,1)	−4.3160; 0.2248	−4.222; 0.340	0.4612
(1,6,2)	−4.3160; 0.2248	−4.222; 0.341	0.4615
(1,6,3)	−4.3160; 0.2248	−4.223; 0.340	0.4609
(1,6,4)	−4.3160; 0.2248	−4.222; 0.341	0.4614
(1,7,0)	0.0000; 0.0000	0.000; 0.000	0.4615
(1,7,1)	−4.3160; 0.2248	−4.221; 0.343	0.4621
(1,7,2)	−4.3160; 0.2248	−4.221; 0.342	0.4616
(1,7,3)	−4.3160; 0.2248	−4.221; 0.342	0.4618
(2,1,0)	0.0000; 0.0000	0.000; 0.000	0.4391
(2,1,1)	−4.3160; 0.2248	−4.259; 0.292	0.4395
(2,1,2)	−4.3160; 0.2248	−4.258; 0.293	0.4398
(2,2,0)	0.0000; 0.0000	0.000; 0.000	0.4532
(2,2,1)	−4.3160; 0.2248	−4.236; 0.322	0.4534
(2,3,0)	0.0000; 0.0000	0.000; 0.000	0.4602
(2,3,1)	−4.3160; 0.2248	−4.224; 0.338	0.4603
(2,3,2)	−4.3160; 0.2248	−4.224; 0.339	0.4604
(2,3,3)	−4.3160; 0.2248	−4.224; 0.338	0.4603
(2,4,0)	0.0000; 0.0000	0.000; 0.000	0.4635
(2,4,1)	−4.3160; 0.2248	−4.218; 0.346	0.4635
(2,4,2)	−4.3160; 0.2248	−4.218; 0.346	0.4635
(2,4,3)	−4.3160; 0.2248	−4.217; 0.348	0.4641
(2,4,4)	−4.3160; 0.2248	−4.218; 0.346	0.4636
(2,4,5)	−4.3160; 0.2248	−4.218; 0.347	0.4637
(2,4,6)	−4.3160; 0.2248	−4.218; 0.346	0.4635
(2,5,0)	0.0000; 0.0000	0.000; 0.000	0.4665
(2,5,1)	−4.3160; 0.2248	−4.212; 0.354	0.4666
(2,6,0)	0.0000; 0.0000	0.000; 0.000	0.4727
(2,6,1)	−4.3160; 0.2248	−4.200; 0.371	0.4732
(2,6,2)	−4.3160; 0.2248	−4.200; 0.372	0.4734
(2,6,3)	−4.3160; 0.2248	−4.201; 0.370	0.4730
(2,6,4)	−4.3160; 0.2248	−4.200; 0.371	0.4733
(2,7,0)	0.0000; 0.0000	0.000; 0.000	0.4740
(2,7,1)	−4.3160; 0.2248	−4.198; 0.374	0.4745
(2,7,2)	−4.3160; 0.2248	−4.198; 0.373	0.4741
(2,7,3)	−4.3160; 0.2248	−4.198; 0.374	0.4743

References

[1] M.H.J. Bollen, A. Sannino, Voltage control with inverter-based distributed generation, IEEE Trans. Power Deliv. 20 (2005) 519–520, https://doi.org/10.1109/TPWRD.2004.834679.

[2] C. Reese, C. Buchhagen, L. Hofmann, Voltage range as control input for OLTC-equipped distribution transformers, PES T&D (2012) 1–6, https://doi.org/10.1109/TDC.2012.6281619.

[3] E. Demirok, P.C. González, K.H.B. Frederiksen, D. Sera, P. Rodriguez, R. Teodorescu, Local reactive power control methods for overvoltage prevention of distributed solar inverters in low-voltage grids, IEEE J. Photovolt. 1 (2) (2011) 174–182, https://doi.org/10.1109/JPHOTOV.2011.2174821.

[4] R. Caldon, M. Coppo, R. Turri, Distributed voltage control strategy for LV networks with inverter-interfaced generators, Electr. Power Syst. Res. 107 (2014) 85–92, https://doi.org/10.1016/j.epsr.2013.09.009.

[5] Y. Bae, et al., Implemental control strategy for grid stabilization of grid-connected PV system based on german grid code in symmetrical low-to-medium voltage network, IEEE Trans. Energy Convers. 28 (3) (2013) 619–631, https://doi.org/10.1109/TIA.2018.2869104.

[6] P. Esslinger, R. Witzmann, Improving grid transmission capacity and voltage equality in low-voltage grids with a high proportion of distributed power plants, Proceedings of the International Conference on Smart Grid and Clean Energy Technologies, Chengdu, China, 2011, pp. 294–302 vol. 12.

[7] B. Bletterie, S. Kadam, R. Bolgaryn, A. Zegers, Voltage control with PV inverters in low voltage networks — in depth analysis of different concepts and parameterization criteria, IEEE Trans. Power Syst. 32 (1) (2017) 177–185, https://doi.org/10.1109/TPWRS.2016.2554099.

[8] M. Nijhuis, M. Gibescu, J.F.G. Cobben, Incorporation of on-load tap changer transformers in low-voltage network planning, IEEE PES Innovative Smart Grid Technologies Conference Europe (ISGT-Europe) (2016) 1–6, https://doi.org/10.1109/ISGTEurope.2016.7856207.
[9] A.R. Malekpour, A. Pahwa, Reactive power and voltage control in distribution systems with photovoltaic generation, North American Power Symposium (NAPS), (2012), pp. 1–6.
[10] A. Ciocia, et al., Voltage control in low-voltage grids using distributed photovoltaic converters and centralized devices, IEEE Trans. Ind. Appl. 55 (1) (2019) 225–237, https://doi.org/10.1109/TIA.2018.2869104.
[11] Technical Guideline — Guideline for generating plants' connection to and parallel operation with the medium-voltage network, June 2008. http://electrical-engineering-portal.com/res2/Generating-Plants-Connected-to-the-Medium-Voltage-Network.pdf.
[12] IEEE Standard for Interconnection and Interoperability of distributed Energy Resources with Associated Electric Power Systems Intefaces, IEEE Std 1547™-2018, pp. 1–137. (Approved 15 February 2018). http://ieeexplore.ieee.org/stamp/stamp.jsp?tp=&arnumber=6879213&isnumber=6879212.
[13] K. Turitsyn, P. Sulc, S. Backhaus, M. Chertkov, Options for control of reactive power by distributed photovoltaic generators, Proc. IEEE 99 (6) (2011) 1063–1073, https://doi.org/10.1109/JPROC.2011.2116750.
[14] P. Jahangiri, D.C. Aliprantis, Distributed Volt/var control by PV inverters, IEEE Trans. Power Syst. 28 (3) (2013) 3429–3439, https://doi.org/10.1109/TPWRS.2013.2256375.
[15] N. Karthikeyan, B.R. Pokhrel, J.R. Pillai, B. Bak-Jensen, Coordinated voltage control of distributed PV inverters for voltage regulation in low voltage distribution networks, 2017 IEEE PES Innovative Smart Grid Technologies Conference Europe (ISGT-Europe) (2017) 1–6, https://doi.org/10.1109/ISGTEurope.2017.8260279.
[16] J.W. Smith, W. Sunderman, R. Dugan, B. Seal, Smart inverter Volt/var control functions for high penetration of PV on distribution systems, 2011 IEEE/PES Systems Conference and Exposition (2011) 1–6, https://doi.org/10.1109/PSCE.2011.5772598.
[17] O. Marggraf, et al., U-control — analysis of distributed and automated voltage control in current and future distribution grids, International ETG Congress (2017) 1–6.
[18] F. Zhang, et al., The reactive power voltage control strategy of PV systems in low-voltage string lines, 2017 IEEE Manchester PowerTech (2017) 1–6, https://doi.org/10.1109/PTC.2017.7980995.
[19] S. Hashemi, J. Østergaard, Methods and strategies for overvoltage prevention in low voltage distribution systems with PV, IET Renew. Power Gener. 11 (2) (2017) 205–214, https://doi.org/10.1049/iet-rpg.2016.0277.
[20] C. Winter, et al., Harnessing PV inverter controls for increased hosting capacities of smart low voltage grids: recent results from Austrian research and demonstration projects, 4th International Workshop on Integration of Solar Power into Power System (2014).
[21] M. Juamperez, G. Yang, S.B. Kjaer, Voltage regulation in LV grids by coordinated volt-var control strategies, J. Mod. Power Syst. Clean Energy 2 (2014) 319–329, https://doi.org/10.1007/s40565-014-0072-0.
[22] A. Cagnano, E. De Tuglie, M. Bronzini, Multiarea voltage controller for active distribution networks, Energies 11 (2018) 583, https://doi.org/10.3390/en11030583.
[23] D.-L. Schultis, A. Ilo, C. Schirmer, Overall performance evaluation of reactive power control strategies in low voltage grids with high prosumer share, Electr. Power Syst. Res. 168 (2019) 336–349, https://doi.org/10.1016/j.epsr.2018.12.015.
[24] R. Tonkoski, L.A.C. Lopes, Impact of active power curtailment on overvoltage prevention and energy production of PV inverters connected to low voltage residential feeders, Renew. Energy 36 (December (12)) (2011) 3566–3574, https://doi.org/10.1016/j.renene.2011.05.031.
[25] IEEE Task Force on Interfacing Techniques for Simulation Tools, Interfacing power system and ICT simulators: challenges, state-of-the-Art, and case studies, IEEE Trans. Smart Grid 9 (January (1)) (2018) 14–24, https://doi.org/10.1109/TSG.2016.2542824.
[26] A. Ilo, 'Link'— the smart grid paradigm for a secure decentralized operation architecture, Electr. Power Syst. Res. 131 (2016) 116–125, https://doi.org/10.1016/j.epsr.2015.10.001.
[27] A. Ilo, D.-L. Schultis, C. Schirmer, Effectiveness of distributed vs. concentrated volt/var local control strategies in low-voltage grids, Appl. Sci. Basel (Basel) 8 (2018) 1382, https://doi.org/10.3390/app8081382.
[28] A. Ilo, Demand response process in context of the unified LINK-based architecture, in: Jean-Luc Bessède (Ed.), Eco-Design in Electrical Engineering- Eco-Friendly Methodologies, Solutions and Example for Application to Electrical Engineering, 1st ed., Springer-Verlag, Berlin/Heidelberg, Germany, 2017, pp. 75–85 ISBN 978-3-319-58171-2.
[29] A. Bokhari, et al., Experimental determination of the ZIP coefficients for modern residential, commercial, and industrial loads, IEEE Trans. Power Deliv. 29 (3) (2014) 1372–1381, https://doi.org/10.1109/TPWRD.2013.2285096.
[30] A. Ilo, Effects of the reactive power injection on the grid — the rise of the volt/var interaction chain, Smart Grid Renew. Energy 7 (7) (2016) 217–232, https://doi.org/10.4236/sgre.2016.77017.